Development of a wavelength-shifting fibre gamma camera

A. J. Soares[1,2], I. Cullum[3], D. J. Miller[2], G .J. Royle[1], R. D. Speller[1]
[1]Dept. Medical Physics and Bioenegineering, University College London
[2]Dept. Physics and Astronomy, University College London
[3]Institute of Nuclear Medicine, Middlesex Hospital, University College London

Abstract

A wavelength-shifting fibre (WSF) gamma camera was built and tested. A spatial resolution of 3.5 mm $\sim$ 4 mm FWHM was achieved which is comparable to that of modern Anger cameras. Two CsI(Na) crystals were tested and both showed lower light output than expected. Hence a poor energy resolution of 23% FWHM was obtained. Simulation results predict a spatial resolution better than 3 mm if the WSF signals are three times higher than those obtained experimentally. Ways of achieving this goal are discussed.

I. INTRODUCTION

Over the last four decades the Anger camera has been the standard imaging device for single photon radio-isotope imaging in nuclear medicine examinations. Among its most relevant performance characteristics for 140 keV gamma rays (from Tc^{99m}) are an intrinsic spatial resolution of 3 $\sim$ 3.5 mm FWHM and an energy resolution of 10% FWHM. Due to their bulky and heavy design, it is often difficult to position the camera to obtain the most favorable imaging projection. Moreover, they have a dead zone at the edges of about 5 cm, which also impairs a correct positioning in some applications, particularly when imaging small organs as, for example, in scintimammography.

We are developing a small gamma camera where the position of interaction of gamma rays in a scintillation crystal is obtained by measuring the profiles of light trapped inside wavelength-shifting fibres (WSF) coupled to the crystal [1, 2]. Our aim is to build a small gamma camera with at least similar performance to that of the Anger camera, having an active area with dimensions close to the size of the detector head. This design also provides flexibility for the choice of the size and shape of the camera to suit a particular application. In our previous studies [1] we evaluated the amount of light trapped in each fibre and the results confirm the feasibility of the concept of a WSF gamma camera, despite the small amount of light trapped in each fibre for a given 140 keV gamma ray interaction (10 $\sim$ 15 photons). In this present work we shall describe the construction and evaluation of a WSF gamma camera prototype. The performance is described in terms of spatial resolution, energy resolution, detection efficiency and position linearity. We also present Monte Carlo simulations studies based on the experimental results obtained, in order to predict further performance improvements.

II. TEST PROTOTYPE

Two different CsI(Na) crystals with 5 $\times$ 5 in^2 area were used [3]. They are 3 and 5 mm thick, which provides a good localisation of the light, for a stopping power similar to 5 mm and 8 mm of NaI(Tl) for 140 keV gamma rays (Anger cameras usually have a 9 mm NaI(Tl) crystal for 140 keV).

Figure 1 shows a schematic diagram of the prototype. Two ribbons of blue-to-green wavelength-shifting fibres (WSFs) are coupled with silicon optical compound to opposite sides of a CsI(Na) slab. The fibre ribbons are placed orthogonally to each other to provide two dimensional position information. For all measurements, we associate the WSF layer coupled to the gamma ray entrance surface (top surface) with the x coordinate (WSF-X) and the bottom layer with the y (WSF-Y). Following a gamma ray interaction in the crystal, light is isotropically emitted. The emission peak of CsI(Na) is at 420 nm. A fraction of this light is absorbed by the fibres (absorption peak at 420 nm - *blue*) and is followed by isotropic emission at a longer wavelength (emission peak at 500 nm - *green*). The *green* photons may be trapped inside the fibres depending on the angle between the fibre axis and the direction of re-emission. The fibres (Bicron BCF-91A [4]) are double cladded with 1 mm diameter circular cross-section and 5.6% trapping efficiency. In order to cover the entire crystal surfaces, we coupled 128 fibres to each side of the crystal. The WSF signals are readout by muti-anode PMTs (see sub-section A) and the position of the gamma ray interaction is estimated by a centroid calculation. The energy signal is obtained by the 2 $\times$ 2 array of closely packed 3" square PMTs (Philips X3392) shown in the figure. The bottom layer of WSFs is coupled to one side of a 5 mm thick perspex slab and the 4 energy PMTs (E-PMTs) are coupled to the other side of the slab. Both couplings are done with silicon optical compound. The E-PMTs operated at -1000 V corresponding to a gain of $\approx$ 2.5 $\times$ 10^5 according to the typical gain curves from the manufacturer's data sheets [7].

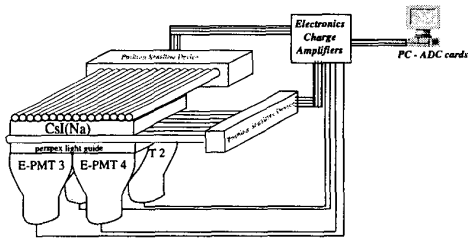

Figure 1: Schematic layout of the WSF gamma camera prototype built and tested.

A. WSF readout sensors

We have evaluated two Hamamatsu [5] R5900-M16 multi-anode PMTs (MA-PMT) for response uniformity

between pixels at low light levels. The R5900-M16 has external dimensions of 28 × 28 mm^2 and an effective entrance window area of 20 × 20 mm^2. The anodes are arranged in a square array of 4 × 4 pixels, each with an area of 4.5 × 4.5 mm^2 and an inter-pixel spacing of 0.5 mm. The dynode structure is a twelve stage metal-channel system, which provides high gain and low cross talk. The two tubes used in the prototype were operated at -1000 V under very stable conditions, yielding a gain of above 10^7, which resulted in very good separation between the pedestal and the single photo-electron peak. The results of the evaluation were presented elsewhere [6] and show that these MA-PMTs are suitable for the readout of the WSFs in this application, despite the low quantum efficiency of the bialkali photocathode ($\approx$ 12% at 500 nm). They both have good single electron resolution and inter-pixel cross-talk of less than 1%. As to the uniformity of response, we are particularly interested in the mean number of photo-electrons collected by the first dynode. We found that within each pixel, there is a 3 × 3 mm^2 region centered in the pixel in which the variations of response are of less than 10% for both tubes. Between different pixels, we found variations of 5% for one tube (used for the x direction) and of 30% for the other (y) tube. The non-uniformity in gain is corrected with variable gain amplifiers. Using two R5900-M16 tubes, we are able to connect 16 fibres in each direction to each tube, or 32 if we couple two fibres per pixel, which can easily be done due to the large area of each pixel. For this reason, of the total 256 fibres covering the entire area of the crystal, a sub-set of 64 fibres were specially cut in 30 cm long pieces with both ends polished following identical procedures. Since we only read-out one end of each fibre, the other end was aluminised to improve light collection at the MA-PMTs. Figure 2 shows the relative positions of the E-PMTs, the scintillation crystal and the fibres in our prototype.

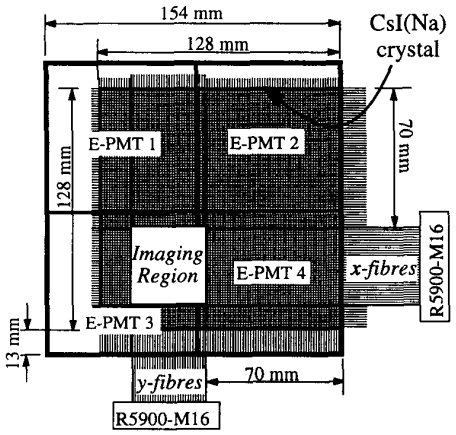

Figure 2: Diagram of a top view of the set-up. It shows the relative positions of the E-PMTs, the scintillation crystal and the fibres.

B. Data acquisition system

A complete data acquisition system was purposely designed and built for this work. The signals from the MA-PMT anodes are amplified in individual charge amplifiers with 5.6 μs shaping time, followed by a variable gain linear amplifier. There are 27 amplifier channels (13 for the WSF-X fibres and 14 for the WSF-Y fibres. The signals from the E-PMTs were amplified similarly in four separate channels. All the amplified signals are digitised in two 16-channel ADC boards connected to a PC via the PCI bus. The four amplified energy signals are summed in a standard summing circuit based on an operational amplifier (*hardware energy sum*) to obtain the total energy signal, which is also digitised using the last available ADC channel. Moreover, the summed signal is connected to a discriminator in order to produce the trigger required for the ADCs. The KmaxNT [8] data acquisition software was used to read-out the ADCs, for image display and for data storage.

III. Methods

Unless otherwise mentioned, the evaluation of the detector performance was carried out using a collimated beam of Co^{57} gamma rays (predominantly 122 keV). For the gamma ray collimation we used a block of lead, 13 mm thick, with a 1 mm diameter hole. Two types of system were tested and compared. In the first one, there was a single WSF coupled to each MA-PMT pixel. The imaging field of view is 13 × 14 mm^2. In the second, two WSF are coupled to each MA-PMT pixel. The imaging field of view is 26 × 28 mm^2. This layout would be preferred to cut down the number of read-out channels. Also, as mentioned above, two crystals with different thickness (3 mm and 5 mm) were tested and compared.

A. Number of photo-electrons per WSF

In order to measure the signals on the WSFs for a given position of the gamma ray source, we calculate the number of photo-electrons produced on the MA-PMTs. Observing the pulse height spectra for fibres near the gamma rays position of interaction, we conclude that the light levels are very low. Therefore, assuming Poisson statistics for the production of photo-electrons, the mean number of photo-electrons, μ, can be calculated by counting the number of zeros, N_{zeros}, in the pedestal. The mean is obtained from $\mu = -ln(N_{zeros} \div N_{total})$, where N_{total} is the total number of triggers in a given window centered around the energy peak.

Figure 3 shows the pulse height spectra for a WSF-X fibre (numbered 8) and for a WSF-Y fibre (numbered 9) for gamma rays interacting near them (within ± 1 mm). In this case, there is a single fibre coupled to each pixel of the MA-PMT. The good separation between the pedestal and the single photo-electron peak can be observed. The MA-PMT reading-out the x fibres layer has a better single electron resolution than the one reading-out the y fibres.

B. Energy response

Two different methods of obtaining the energy signal were compared. Firstly, the digitised signals of the four E-PMTs were summed and the corresponding pulse height distribution was recorded. It was compared to the pulse height distribution for the *hardware energy sum* and it is found to contain very

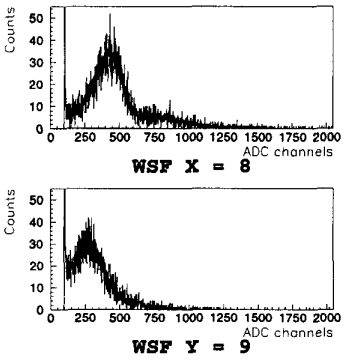

Figure 3: Pulse height spectra for a WSF-X fibre and for WSF-Y fibre. The mean number of photo-electrons is 0.5 for WSF-X fibre and 0.4 for the WSF-Y fibre.

similar information (same FWHM for the 122 keV peak). Thus, all further references to the energy signal refer to the *hardware energy sum* pulse height distribution. An energy window was selected around the 122 keV peak to discard unwanted trigger events. Figure 4 shows the energy pulse height distribution for a collimated beam of gamma rays. A poor energy resolution of 23% FWHM is obtained which is explained in more detail in section IV. A.

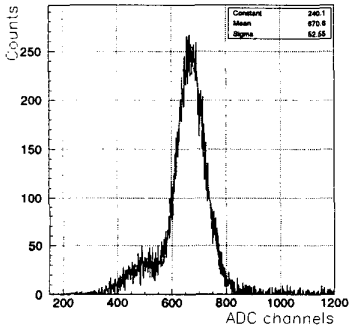

Figure 4: Energy spectrum for Co^{57} gamma rays. The collimated beam of gamma rays is located above the central *imaging region* shown in figure 2.

C. Images

The x and y coordinates of an event with energy inside the selected window, are found by calculating the centroids of the WSF signals for both directions, as shown in equation 1 where X_i and Y_i are the signals on the i^{th} fibre for each direction.

$$x = \frac{\sum_{i=1}^{m} i.X_i}{\sum_{i=1}^{m} X_i} \quad ; \quad y = \frac{\sum_{i=1}^{m} i.Y_i}{\sum_{i=1}^{m} Y_i} \qquad (1)$$

For the case of a single WSF coupled to each MA-PMT pixel, the index i takes consecutive values from 1 to 13 for x and from 1 to 14 for y. For two fibres per pixel, i takes only odd numbers from 1 to 25 for x and from 1 to 27 for y, since each imaging pixel is now 2 mm wide.

IV. Results

A. The energy signal

1) Energy resolution

Before assembling the prototype with the WSFs, the energy response of both CsI(Na) crystals was measured directly coupled to the perspex slab with silicon optical compound, with the four E-PMTs coupled to the opposite side of the slab as in figure 1. All the other surfaces of the crystals were left uncovered. The highest signal was observed when the collimated beam of gamma rays was located above the central regions of E-PMT 2 and E-PMT 4 (see figure 2), with a corresponding energy resolution of 19% FWHM for both crystals. This value is very high compared to the energy resolution achieved with NaI(Tl) crystals (10%). According to tabulated values of light yield of scintillators [9], CsI(Na) and NaI(Tl) should have very similar light yields and almost identical emission spectra, which indicates that the CsI(Na) crystals used had poor light yield. After introducing the fibres, the energy signal dropped to about 60% of the above results, with a subsequent worsening in energy resolution to 23% FWHM. This relatively small reduction in the energy signal when the WSFs are introduced is a very encouraging result. With brighter crystals, Anger cameras achieve 10% energy resolution, thus, we expect that overall values of 13% ~ 14% can be achieved after the WSFs are introduced.

2) Energy uniformity

The uniformity of the energy signal was also evaluated and the results are shown in figure 5, for the 3 mm thick crystal. The points indicated in the figure correspond to the highest energy signals, obtained at the central regions of the E-PMTs as well as to the lowest ones, at the E-PMTs' edges or at the edges of the crystals. The highest difference in peak position for the points shown is 30%.

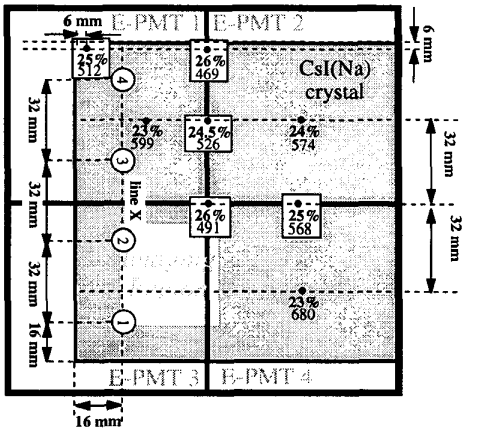

Figure 5: Energy uniformity map for a few points across the area of the camera. Values in bold correspond to energy resolution, while the values below these correspond to the position of the peak in arbitrary units.

B. *Imaging performance*

The imaging behaviour of the prototype was evaluated for four configurations, depending on the thickness of the crystal (3 mm or 5 mm) and on the sampling pitch (1 mm or 2 mm), i.e., whether one or two fibres were coupled to each MA-PMT pixel. The following results refer to the 3 mm thick CsI(Na) and 1 mm sampling pitch. The fibres are labeled WSF-X1 to WSF-X13 for the x direction and WSF-Y1 to WSF-Y14 for y. A summary of the results for the other cases is shown in table 1 for comparison.

1) Spatial resolution

Figure 6 shows the image obtained for a collimated beam of Co^{57} gamma rays, with 35,000 events inside energy window.

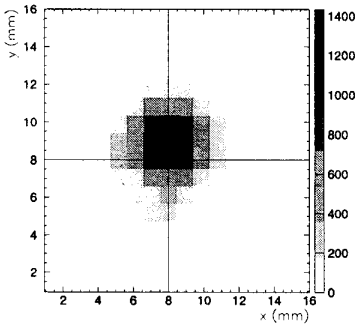

Figure 6: Image of the collimated beam of Co^{57} gamma rays. The collimator hole is located approximately above WSF-X8 and WSF-Y9.

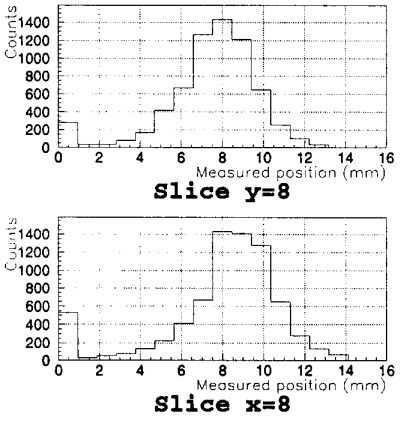

Figure 7: Profiles along the lines drawn in figure 6. A spatial resolution of 4 mm FWHM is obtained for both the x and the y directions.

Analysis of the profiles across the highest intensity pixel (figure 7) show a spatial resolution of 4 mm FWHM for both the x and y directions The mean values of the profiles are 8.3 and 8.7 for x and y respectively. For the fibres located directly under the collimator hole, a mean number of photo-electrons of 0.5~0.6 was observed. The total number of photo-electrons in the 13 WSF-X fibres was 3.3 and for the 14 WSF-Y fibres it was 2.8. This corresponds to very low statistics for the centroid calculations. Thus, the spatial resolution is mainly determined by the light spread over the WSF planes, which is of the order of the thickness of the crystal.

2) Position linearity

To study the position linearity of the device in both directions, the lead collimator was positioned at successive points along two lines parallel to either x or y. The points were separated by 1 mm, and the positioning accuracy of the collimator hole is estimated to be of the order or ± 0.5 mm. The mean values of the profile distributions are plotted against the true collimator position in figure 8 for each case, showing the linearity of the position reconstruction.

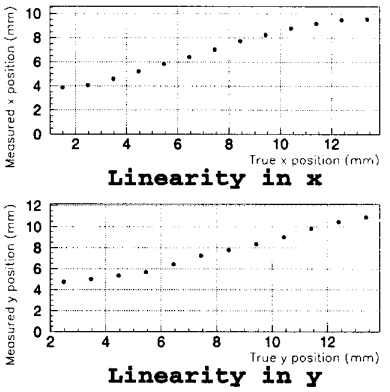

Figure 8: Linearity plots for two lines: one parallel to x and the other parallel to y.

C. *Imaging efficiency*

Due to the very low light levels at the WSFs, there are some cases where, for a trigger event falling inside the energy window, there are zero photo-electrons in the WSF-X fibres or the WSF-Y fibres or both. These cases do not produce valid image points and therefore decrease the overall counting efficiency of the detector. Taking the points shown in figure 8, the average percentage of non-valid events is found to be 7% $\pm$ 1.3%, which does not represent a significant efficiency loss. Furthermore, the light output of this crystal is lower than expected, as discussed in section A, and by using a brighter crystal the percentage of these non-valid imaging events will become even less relevant. We call this efficiency parameter the *imaging efficiency* of the device.

D. *Comparison between the 4 configurations*

Similar assessment was carried out for the the other three configurations described in section B and the results are summarized in table 1. The ranges of values for the spatial resolution refer to the results obtained at different locations of the lead collimator. The variations in light output from different fibres possibly accounts for such spatial resolution fluctuations.

V. Monte Carlo simulation

A Monte Carlo simulation code was previously developed [1] to model the output of a photomultiplier tube

Table 1
Imaging performance characteristics

Crystal thickness	Sampling pitch	Spatial resolution FWHM	Imaging efficiency
3 mm	1 mm	3.5 mm ~ 4 mm	≥ 90%
3 mm	2 mm	5 mm ~ 6 mm	≥ 90%
5 mm	1 mm	4 mm ~ 6 mm	≥ 90%
5 mm	2 mm	5 mm ~ 8 mm	≥ 90%

in the photon counting region. For a given mean number of photo-electrons, it randomly samples the number of photo-electrons from a Poisson distribution. The subsequent charge multiplication process is described by a gaussian distribution whose rms is the single electron resolution of the tube. Since we can calculate the mean number of photo-electrons for each fibre and we know the single electron resolution of the MA-PMTs used, we can simulate the imaging performance and compare to the experiments. The comparison was made for the data shown in figure 6. The mean number of photo-electrons in each fibre was calculated and used as input for the simulation program. An image was obtained which agreed very well with the experimental data (figure 6). Then, the previous number of photo-electrons was multiplied by two and by three and used as input in our simulation. The spatial resolution improved to 3.2 mm and 2.8 mm respectively. An increase in the number of photo-electrons can realistically be achieved by the use of a brighter sample of CsI(Na) or NaI(Tl), or replacing the MA-PMTs with silicon based devices, like Avalanche Photo-Diodes (APD) or Visible Light Photon Counters (VLPC), which have quantum efficiency 3 or 4 times higher at 500 nm than any PMT photocathode. We are therefore optimistic that a spatial resolution better than the Anger camera can be achieved with currently available technology.

VI. Summary and Conclusions

A WSF gamma camera prototype was built and tested. Its imaging capabilities were demonstrated for Co^{57} gamma rays. Despite the low light output of the scintillation crystal used, a spatial resolution of 3.5 mm ~ 4 mm FWHM was achieved which is comparable to the 3.5 mm intrinsic resolution of the Anger camera. The energy resolution obtained was 22 ~ 23% FWHM. This poor result is due to the low light output of the CsI(Na) samples available. The energy signal of the WSF prototype was 60% compared to the signal obtained for a direct coupling of the crystal to the PMTs. On this basis we predict an improvement in energy resolution to 14% or less if using a brighter sample of scintillator or with NaI(Tl). The imaging efficiency, defined as the ratio between the counts in the useful area in the image to the total counts in the energy window, is found to be greater than 90%.

A Monte Carlo simulation predicts improvement to 3.2 mm and 2.8 mm FWHM in spatial resolution if the WSF signals are two or three times higher than those found in this prototype. This can be achieved by the use of brighter scintillator samples (or NaI(Tl)) or using silicon based devices such as APDs or VLPCs for the WSF read-out.

VII. Acknowledgments

The authors would like to thank Dr. Stan Majewski and Dr. Drew Weisenberger from the Thomas Jeffreson National Accelerator Facility, for supplying the KmaxNT software and for help in the data acquisition code. Thanks are also due to Dr. Jenny Thomas, University College London, for help and advise on the evaluation of the R5900-M16.

A. J. Soares is funded by Fundação para a Ciência e a Tecnologia (ref. PRAXIS XXI/BD/5133/95), Portugal.

VIII. References

[1] A. J. Soares, I. Cullum, D. J. Miller, G. J. Royle, R. D. Speller "Development of a small gamma camera using wavelength-shifting fibres coupled to inorganic scintillation crystlas for imaging 140 keV gamma rays," *IEEE Trans. Nucl. Sci., NS-34(1), 1999* pp. 23–25

[2] W. Worstell, O. Johnson, H. Kudrolli and V. Zavarzin, "First Results with HighResolution PET Detector Modules using WavelengthShifting Fibers", *IEEE Nuclear Science Symposium Conference Record, November 915, Albuquerque, New Mexico, USA, 1997.*

[3] The CsI(Na) crystals were manufactured by Hilger Crystals, Westwood, Margate, Kent CT9 4JL, United Kingdom.

[4] The wavelengthshifting fibres were manufactured by Bicron, 12345 Kinsman Rd., Newbury, Ohio 440659577, USA.

[5] The R5900-M16 were manufactured by Hamamatsu Photonics K.K., Electron Tube Center, 314-5, Shimokanzo, Toyooka-village, Iwata-gun, Shizuoka-ken, 438-01, Japan.

[6] A. J. Soares, I. Cullum, D. J. Miller, G. J. Royle, R. D. Speller "Photon counting with the Hamamatsu H6568 multi-anode photomultiplier," *presented at the 5^{t}h Position Sensitive Detectors conference, London, September 1999.*

[7] The X3392 photomultipliers (E-PMTs) used were manufactured by Photonis *imaging sensors*, France.

[8] KmaxNT is supplied by Sparrow Coorporation, USA.

[9] G. F. Knoll, "Radiation detection and measurement", 2nd Ed., John Wiley & Sons, 1988.